ACS APPLIED MATERIALS & INTERFACES

Research Article

www.acsami.org

# $PbI_2$-Based Dipping-Controlled Material Conversion for Compact Layer Free Perovskite Solar Cells

Enqiang Zheng,[†] Xiao-Feng Wang,[*,†] Jiaxing Song,[§] Lulin Yan,[§] Wenjing Tian,[*,§] and Tsutomu Miyasaka[‡]

[†]Key Laboratory of Physics and Technology for Advanced Batteries, Ministry of Education, College of Physics, and [§]State Key Laboratory of Supramolecular Structure and Materials, Jilin University, Changchun 130012, PR China

[‡]Graduate School of Engineering, Toin University of Yokohama, 1614 Kurogane-cho, Aoba, Yokohama, Kanagawa 225-8503, Japan

**ABSTRACT:** A two-step sequential deposition method has been extensively employed to prepare the $CH_3NH_3PbI_3$ active layer from the $PbI_2$ precursor in perovskite solar cells (PSCs). The variation of the photovoltaic performance of PSCs made by this method was always attributed to different dipping times that induce complete/incomplete conversion of $PbI_2$ into $CH_3NH_3PbI_3$. To solve this issue, we employed a solvent vapor annealing (SVA) method to prepare $PbI_2$ crystallites with large grain size for preparation of high quality perovskite. With this method, the increased $PbI_2$ dipping time in $CH_3NH_3I$ solution was found to reduce the photovoltaic performance of resulting PSCs without a significant change in $PbI_2/CH_3NH_3PbI_3$ contents in the perovskite films. We attribute this abnormal reduction of the photovoltaic performance to intercalation/deintercalation of the $PbI_2$ core with a $CH_3NH_3PbI_3$ shell, which causes the doping effect on both the $PbI_2$ and $CH_3NH_3PbI_3$ crystal lattices and the formation of a $CH_3NH_3PbI_3$ capping layer on the surface, as revealed by UV−vis absorption, X-ray diffraction, FT-IR, and scanning electron microscope measurements. Based on our findings, a multistep dipping-drying process was employed as an alternative method to improve the crystalline quality. The method achieved power conversion efficiency up to 11.4% for the compact layer free PSC sharing a simple device structure of ITO/perovskite/spiro-OMeTAD/Ag.

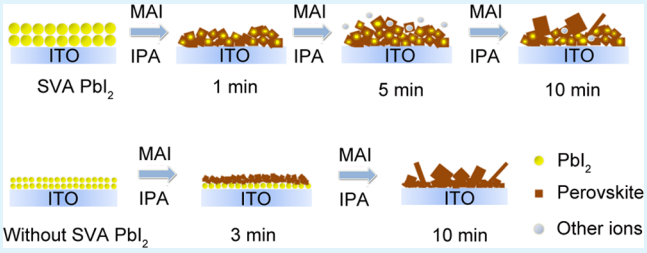


**KEYWORDS:** *perovskite solar cells, compact layer free, solvent vapor annealing, low-temperature-processed device, $PbI_2$ intercalation*

## INTRODUCTION

In the last five years, perovskite solar cells (PSCs) have attracted considerable attention because of their cost-effectiveness, ease of fabrication, and excellent photovoltaic performance.[1−7] To date, the power conversion efficiency (PCE) of the best fabricated PSC has reached ∼20%.[8] This PCE is comparable with the commercially available multicrystal silicon solar cells. The high PCE is attributed to the excellent optoelectrical properties of perovskite materials, e.g., high extinction coefficient, long charge carrier diffusion length, and superior ambipolar carrier transport ability.[9−11] Although PSCs were typically constructed with both electron- and hole-transporting layers for efficient charge carrier collection,[12−15] the fact that comparable PCEs were achieved for compact layer free PSCs indicates that the electron-transporting layer other than the indium-doped tin oxide (ITO) conductive substrate is not essential.[16,17] Such a simplified PSC structure is particularly helpful for studying the growth mechanisms of perovskite crystallites free from the interference of the morphology/chemical properties of the underlying semiconductor films.

In fact, efforts have already been devoted to broadening our knowledge about the formation of perovskite films. Numerous processing techniques of perovskite layers have been reported so far, such as one-/two-step solution process, vacuum deposition, and solvent vapor/additive assisted crystal growth.[6,18−23] Obviously, the method of processing the perovskite layer is critical for achieving high efficiency PSCs. Besides the processing method of the perovskite layer, the presence of a $PbI_2$ precursor can also significantly affect the performance of the PSCs device with the two-step sequential deposition method. The improved PCE by remnant $PbI_2$ was mainly attributed to the passivation effect to the interface of the perovskite, because it was found that $PbI_2$ was mainly left in perovskite grain boundaries or at the relevant interfaces, which improves the carrier charge property.[24] However, the $PbI_2$ precursor is not stable, which gradually converts into perovskite during the prolonged dipping process in $CH_3NH_3I$ (MAI) solution.[25] Therefore, the decreased PCE of these PSCs through the prolonged dipping process can be attributed to the vanishing of the $PbI_2$ passivation layer.[24] In view of this, our previous investigation introduced a solvent vapor annealing (SVA) method to the typical two-step sequential deposition method in preparation of PSC cells. By the SVA process, the $PbI_2$ precursor layer becomes highly crystallized and can stably remain in the final perovskite films to develop a passivation effect.[26] Thus, it is expected that such PSCs with a highly

**Received:** June 29, 2015
**Accepted:** July 29, 2015
**Published:** July 29, 2015





DOI: 10.1021/acsami.5b05787
*ACS Appl. Mater. Interfaces* 2015, 7, 18156−18162

crystallized $PbI_2$ layer are robust against the prolonged dipping process, resulting in improved photovoltaic performance with longer dipping time.

In this article, we fabricated compact layer free PSCs with the two-step sequential deposition method, in which the $PbI_2$ precursor layers were prepared both with and without the SVA process. For both cases, the photovoltaic performance of PSCs with varied dipping times was compared. Given that remnant $PbI_2$ is a positive occurrence for photovoltaic performance, PSCs with SVA-processed $PbI_2$ may give improved PCE with increased dipping time. Thus, we address first the question of this article: how does the dipping time affect the photovoltaic performance of PSCs with and without the highly crystallized $PbI_2$ precursor? As the photovoltaic performance may increase/decrease with increased dipping time for PSCs with and without the SVA process, consequently, we examined the perovskite layer with UV−vis absorption spectroscopy, X-ray diffraction (XRD), and FT-IR measurements. We therefore address a second question: what causes the increased/decreased photovoltaic performance with increased dipping time? As an alternative way of increasing the total dipping time, a repeated dipping-drying method was employed to improve the conversion of $PbI_2$ into perovskite. This trial leads to the last question: can the repeated dipping-drying process give improved photovoltaic performance? Our approach to solve these questions by successful control of $PbI_2$-based preparation of perovskite led creation of a compact layer free perovskite capable of high PCE up to 11.4%.

## EXPERIMENTAL SECTION

**Materials.** The lead iodide (beads, −10 mesh, 99.999% trace metals basis) and Li-TFSI (>99.0%) were purchased from Aldrich. The $CH_3NH_3I$ (>99.0%) was purchased from Xi'an Polymer Light Technology Corp. The Spiro-OMeTAD (2,2′,7,7′-tetrakis(*N*,*N*-di-4-methoxyphenylamino)-9,9′-spirobifluorene, >99.0%) was purchased from Merck. The Ultradry solvents *N*,*N*-dimethylformamide (DMF, >99.9%) and isopropanol (>99.9%) were obtained from J&K and Acros, respectively. All the chemicals and solvents were stored in a $N_2$ filled glovebox and used as received.

**Device Fabrication.** The prepatterned ITO glass substrates were cleaned with detergent, deionized water, chloroform, acetone and 2-propanol in sequence. Before spin coating, the substrates were treated by plasma cleaning for 5 min. $PbI_2$ was dissolved in DMF at 70 °C. The concentration of $PbI_2$ solution was 460 mg/mL. Then, the solution was spin-coated on the ITO at 4000 rpm for 30 s. For the solvent vapor annealing process (SVA), a part of $PbI_2$ films was kept in a Petri dish for 10 min exposure to solvent vapor in a DMF vapor environment, allowing a slow growth of large sized $PbI_2$ nanoparticles, as detailed in the previous investigation.[25] This film was subsequently annealed at 70 °C. The other part of $PbI_2$ films was directly annealed without SVA in a Petri dish. After cooling down, the substrates were dipped into a solution of $CH_3NH_3I$ in 2-propanol (10 mg/mL) for different durations (1 min, 3 min, 5 min, 10 min), followed by rinsing with 2-propanol. The film was then dried under a flow of clean air. The hole-transport layer (HTL) containing 80 mg of Spiro-OMeTAD, 46.5 μL of Li-TFSI, and 10.5 μL of 4-*tert*-butylpyridine in 1 mL of chlorobenzene was spin-coated on top of the perovskite film at 4000 rpm for 30 s. Finally, 100 nm of Ag was thermally evaporated on the top of the HTL to form the back contact. For each condition, 10 separated devices were fabricated. The active area of PSCs as defined by a mask was 0.04 $cm^2$.

**Characterization.** The morphologies of the films of perovskite were observed using scanning electron microscopy (SEM, Hitachi SU8020). X-ray diffraction (XRD) was measured using a Rigaku SmartLab X-ray diffractometer with Cu Kα radiation (λ = 1.5418 Å) at 25 °C. J-V curves of perovskite solar cell were recorded using a Keithley 2400 source meter measurement system under an AM1.5G filter at a calibrated incident intensity of 100 mW $cm^{-2}$. The J-V curves were measured from open-circuit to forward bias. IPCE values were measured using a commercial IPCE setup (Crowntech QTest Station 1000AD) in air under short-circuit conditions, which were equipped with a 100W Xe arc lamp, filter wheel, and monochromator. Monochromated light was chopped at a frequency of 80 Hz and photocurrents measured using a lock-in amplifier. UV−vis spectra were recorded on a Shimadzu UV-2550 spectrophotometer. The Fourier transform infrared (FT-IR) spectrum was measured with a Bruker VERTEX 80 V FT-IR spectrometer in the range 4000−400 $cm^{-1}$ at room temperature.

## RESULTS AND DISCUSSION

**Dependence of Photovoltaic Performance on the Dipping Time for PSCs with and without the SVA Process.** Although there are conflict debates on the issue of $PbI_2$ remaining in the perovskite layers,[10,27] to the best of our knowledge, a comprehensive comparison was not available before we started this investigation. Therefore, we first prepared the $PbI_2$ precursor films with and without the solvent vapor annealing (SVA) process. Figure 1 shows the XRD patterns and

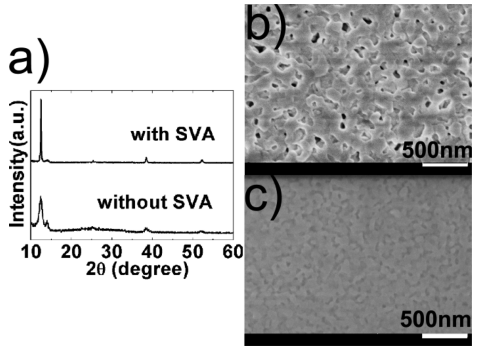


**Figure 1.** (a) XRD diffraction patterns of ITO/$PbI_2$ and (b and c) SEM images of ITO/$PbI_2$ films with SVA (b) and without SVA (c).

scanning electron microscope (SEM) surface images of the $PbI_2$ films obtained both with and without the SVA process. The XRD pattern shows the peak position of the $PbI_2$ films in both cases situated at 12.5° (001) with different full-width-at-half-maximum (fwhm) values. The fwhm of the $PbI_2$ film with SVA is obviously sharper and narrower than that without SVA. We employ the Scherrer formula, i.e. $D = K\lambda/(\beta \cos \theta)$, where D is the grain size of the ordered domains, K is the constant 0.88, λ is the X-ray radiation wavelength (Cu Kα, 1.5406 Å), β is fwhm, and θ is the peak position, to calculate the grain size of the crystallites of the $PbI_2$ nanocrystals in both cases.[28] As a result, the grain size is 41.3 nm for the $PbI_2$ crystals with SVA, whereas the grain size is merely 9.8 nm for $PbI_2$ crystals without SVA. Obviously, SVA substantially induced formation of bigger grains of $PbI_2$. The SEM images of the $PbI_2$ films are consistent with the corresponding XRD results that SVA increases the domain size of the $PbI_2$ film. It was found in the previous investigations that $PbI_2$ forms a large aggregate along the 001 plate, resulting in a surface domain size that is larger than the exact grain size of the $PbI_2$ crystallites.[15,26]

The significant difference between the $PbI_2$ films with and without the SVA process is expected to strongly affect their reactivity with MAI in 2-propanol. The large grain size of $PbI_2$ with SVA may limit the reaction with MAI to occur in the inner part of the grain, resulting in the generation of a $PbI_2$−


DOI: 10.1021/acsami.5b05787
ACS Appl. Mater. Interfaces 2015, 7, 18156−18162

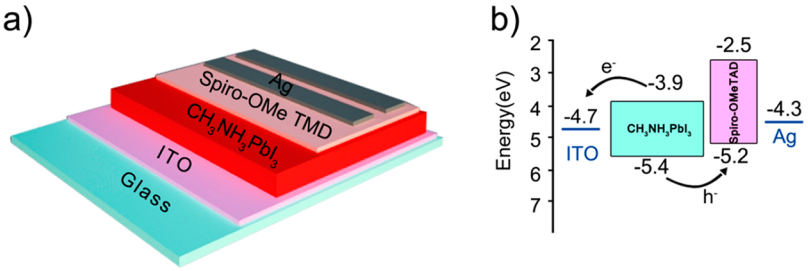


**Figure 2.** (a) Device architecture and (b) energy diagram of the ITO/$MAPbI_3$/spiro-OMeTAD/Ag cells.

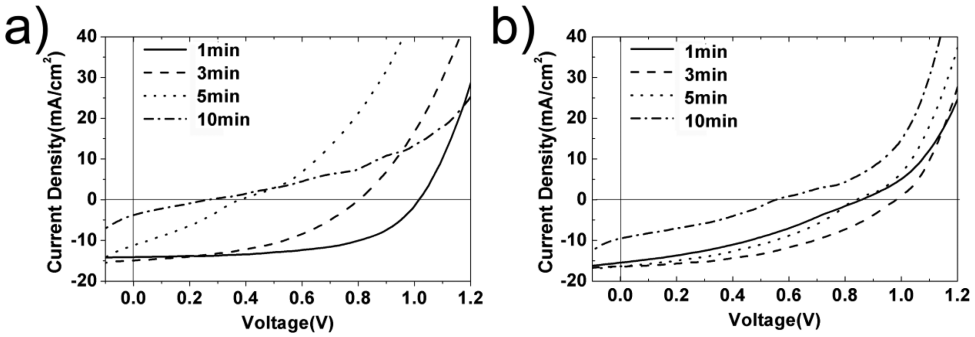


**Figure 3.** J–V curves of the ITO/perovskite/spiro-OMeTAD/Ag devices based on the $PbI_2$ layer with SVA (a) and without SVA (b).

perovskite core–shell structure, as we observed in the previous investigations.[26] This core–shell structure is favorable for fast charge transport in the perovskite film, because the $PbI_2$ core has smaller diffusion length and carrier mobility than the $CH_3NH_3PbI_3$ shell, allowing more charges to transport through the surface perovskite shell with shallow traps.[23] On the other hand, the large grain size of $PbI_2$ with SVA helps diffusion of MAI into the cavities of the film, resulting in the surface of the $PbI_2$ grain being quick transferred into perovskite.

The perovskite active layers were then prepared by dipping these $PbI_2$ precursors with and without the SVA process into MAI solution for different durations of 1, 3, 5, and 10 min. PSCs were then fabricated with these perovskite layers. Figure 2 shows (a) the device structure and (b) the energy alignment of the fabricated PSCs. If metal oxide semiconductor ($TiO_2$, ZnO, and etc.) is employed as the underlying compact layer of the $CH_3NH_3PbI_3$ perovskite, perovskite may easily decompose on the semiconductor surface by photocatalytic reaction. Here, no compact layer was employed in the PSCs of the present investigation. With such a simplified PSC structure, the possible interaction between the compact layer and $PbI_2$/perovskite could also be excluded from the discussion. Figure 3 shows the current density–voltage (J-V) curves of PSCs prepared by a two-step sequential deposition method using the $PbI_2$ precursor with and without SVA. Table 1 and Table 2 show the related parameters of photovoltaic performance obtained from the J-V curves. In the case of $PbI_2$ with SVA, the short-circuit current density ($J_{sc}$) increases from 13.9 mA $cm^{-2}$ to 15.1 mA $cm^{-2}$ with increased dipping time from 1 to 3 min, which was followed by a decrease to 11.3 mA $cm^{-2}$ with the dipping time of 5 min and then significantly drop to 3.5 mA·$cm^{-2}$ with further increasing the dipping time to 10 min. Meanwhile, the open-circuit voltage ($V_{oc}$) and fill factor (FF) are both decreased with increasing the dipping time through 1–10 min. As a result of the varied $J_{sc}$, $V_{oc}$, and FF values, the power conversion efficiency (PCE) reaches the maximum value of 8.4% with the shortest 1 min dipping time. In contrast, without the SVA on $PbI_2$, the photovoltaic performance varies differently in PSCs with increased dipping time. All photovoltaic parameters of PSCs without SVA were essentially low compared to those with SVA. The highest PCE of 7.1% was achieved for PSC with 3 min dipping time of $PbI_2$ in MAI. Thus, in PSCs either with SVA or without SVA, the photovoltaic performance decreases after reaching their highest PCE with further increased dipping time, despite the fact that the variation of the former is more severe.

**Table 1. Photovoltaic Performance of PSCs Based on $PbI_2$ with SVA with Extended Dipping Times**

| Dipping time (min) | $J_{sc}$ (mA/cm²) | $V_{oc}$ (V) | FF | PCE (%) |
|---|---|---|---|---|
| 1 | 13.9 | 1.01 | 0.60 | 8.4 |
| 3 | 15.1 | 0.79 | 0.46 | 5.5 |
| 5 | 11.3 | 0.40 | 0.32 | 1.5 |
| 10 | 3.5 | 0.25 | 0.26 | 0.2 |

**Table 2. Photovoltaic Performance of PSCs Based on $PbI_2$ without SVA with Extended Dipping Times**

| Dipping time (min) | $J_{sc}$ (mA/cm²) | $V_{oc}$ (V) | FF | PCE (%) |
|---|---|---|---|---|
| 1 | 15.5 | 0.83 | 0.36 | 4.7 |
| 3 | 16.2 | 0.97 | 0.45 | 7.1 |
| 5 | 16.2 | 0.86 | 0.41 | 5.7 |
| 10 | 9.5 | 0.54 | 0.35 | 1.7 |

The facilely achievable high PCE at merely 1 min dipping time for the SVA-based PSC is attributable to the big cavities in the $PbI_2$ layer that allow quick reaction of the outer part of $PbI_2$ crystallites with MAI. The significantly dropped PCE with increased dipping time after 1 min, however, is not expected to change. In previous investigations,[25] the dipping time of $PbI_2$ in MAI mainly affects the residue of $PbI_2$ in the perovskite layer. The high efficiency of PSCs prepared by the sequential deposition method was always attributed to either a complete conversion of $PbI_2$ into perovskite or a proper amount of $PbI_2$


DOI: 10.1021/acsami.5b05787
ACS Appl. Mater. Interfaces 2015, 7, 18156–18162

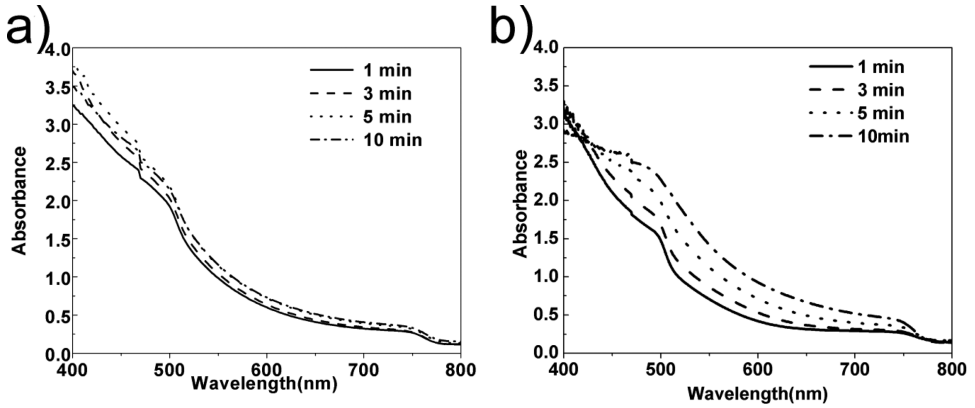


**Figure 4.** UV−vis absorption spectra of $MAPbI_3$ films obtained (a) with SVA and (b) without SVA.

to give a passivation effect. In this investigation, the inner part of large and robust $PbI_2$ crystallites made by the SVA method would require a longer time for their conversion into perovskite, or in other words, the photovoltaic performance of PSCs prepared with the SVA method should be much less insensitive to the prolonged dipping time after reaching the highest values. Thus, the substantially reduced photovoltaic performance of SVA-based PSCs after prolonged dipping time should not be simply attributed to the conversion/decomposition between $PbI_2$ and $MAPbI_3$ perovskite.

**Mechanism of Performance Reduction with Prolonged Dipping Time.** To investigate the factors other than the transformation between $PbI_2/MAPbI_3$ to cause the reduction of the photovoltaic performance of PSCs with increased dipping time, we first pursue examination of the optical properties of the perovskite films. Figure 4 shows the electronic absorption spectra of $MAPbI_3$ films obtained from $PbI_2$ with and without SVA and with different dipping times in MAI. The $PbI_2$ films without SVA exhibit consistently increased absorption intensity over the increased dipping time, owing to the formation of more perovskite products. This observation is in good agreement with a previous investigation.[29] In contrast, the absorption spectra of perovskite films with increased dipping time of SVA-based $PbI_2$ in MAI are more or less similar. Obviously, the light-harvesting ability of the PSCs with SVA is not much affected by the increased dipping duration. Also, it seems that the passivation effect by $PbI_2$ is on a same comparable level, if there is any.

As described above, the $V_{oc}$ values of PSCs with SVA substantially decrease with increased dipping time. This phenomenon seems to be originated from changes in the crystal structure of the perovskite semiconductor. Figure 5 shows the XRD patterns of the perovskite films obtained from $PbI_2$ with SVA (a) and without SVA (b) for different dipping times. In Figure 5a, clear diffraction peaks from perovskite appear at each 14.0°, 24.3°, 28.4°, 31.7°, and 50.3°, corresponding to the (110), (202), (220), (310), and (404) planes of the tetragonal phase of $CH_3NH_3PbI_3$, respectively.[30] Meanwhile, the XRD peak from the $PbI_2$ nanocrystals at 12.56° remains strong throughout the dipping time from 1 to 10 min. In contrast, without the SVA process, the XRD peak at 12.56° in Figure 5b decays significantly with increasing dipping time, and finally disappears after 10 min. The XRD patterns without SVA are also consistent with previous investigations, confirming a nearly complete conversion of $PbI_2$ into $CH_3NH_3PbI_3$ after 10 min. Importantly, as shown in the inset of Figure 5b that

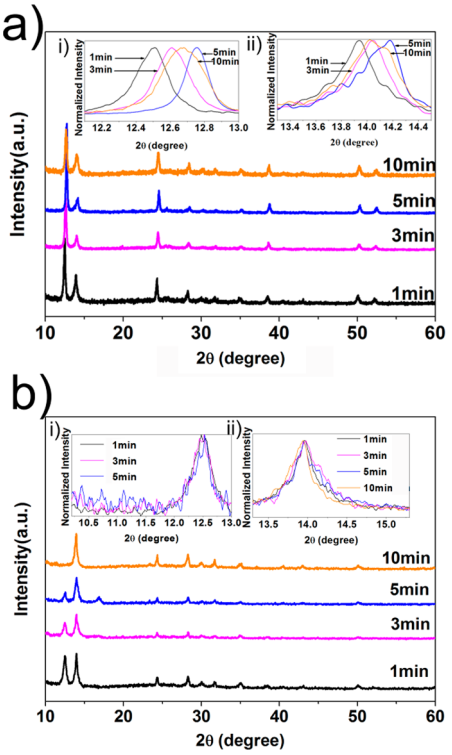


**Figure 5.** XRD diffraction patterns of the ITO/$MAPbI_3$ thin films obtained from $PbI_2$ (a) with SVA and (b) without SVA.

normalizes XRD peaks at 14.0° (001) and 12.56° (110), the XRD peaks for $PbI_2$ and $CH_3NH3PbI_3$ are identical with the peak position, indicating that the crystallite lattices of both $PbI_2$ and $CH_3NH_3PbI_3$ are not altered by long time dipping. Given that the XRD peaks of these $PbI_2$ and $MAPbI_3$ in Figure 5b are identical, their peak positions at 12.56° (001 plane of $PbI_2$) and 14.0° (110 plane of $MAPbI_3$) could be regarded as the intrinsic values for standard $PbI_2$ and $MAPbI_3$ crystals.

On the other hand, interestingly, the normalized peaks of the 001 plane of $PbI_2$ and the 110 plane of $MAPbI_3$ in the inset of Figure 5a shift significantly with the dipping time from 1 to 10 min. The XRD peaks corresponding to the 001 plane of $PbI_2$ are 12.50°, 12.61°, 12.75°, and 12.67°, for dipping times of 1, 3, 5, and 10 min, respectively; meanwhile, the XRD peaks corresponding to the 110 plane of $MAPbI_3$ are 14.0°, 14.1°, 14.2°, and 14.1°, for the dipping times of 1, 3, 5, and 10 min, respectively. Clearly, the peak positions of $PbI_2$ and $MAPbI_3$


DOI: 10.1021/acsami.5b05787
ACS Appl. Mater. Interfaces 2015, 7, 18156−18162

with 1 min dipping time are most close to their intrinsic positions. As the dipping time increases from 1 to 5 min, the XRD peaks shift with the maximum values of 0.25° and 0.2° for $PbI_2$ and $MAPbI_3$, respectively. The shift of XRD peaks within 5 min of dipping time may be a consequence of the coordinate variation of $Pb^{2+}$ and intercalation of interstitial molecules, ions, or atoms forming a transient state.[31] In the other words, the XRD peak shifts of both $PbI_2$ and $MAPbI_3$ crystallites correspond to the doping effect on the perovskite crystals by $PbI_2$ intercalation/deintercalation processes. The optoelectrical properties of both $PbI_2$ and $MAPbI_3$ crystallites will substantially change upon this doping, because excessive MAI ions will disturb the carrier generation/transport in the bulk crystals. Thus, this explains the reductions of $V_{oc}$ and PCE values of SVA-based PSCs with increasing dipping time from 1 to 5 min. This explanation could be further confirmed by FT-IR measurement. Figure 6 shows the FT-IR spectra of the perovskite films prepared by dipping the SVA-based $PbI_2$ in MAI for 1−10 min, and those of pure $PbI_2$ and MAI are also measured as references. The FT-IR signal for 1 min dipping time represents the fully intercalated $PbI_2$ in MAI, and the typical IR shift of $PbI_2$ at wavenumber of 1089 $cm^{-1}$ is not present.[32] As the dipping time increased to 5 min, this IR peak appeared with a disappearance of peaks at 1599 and 3200 $cm^{-1}$, both originated from MAI. Such changes in IR spectra strongly support the hypothesis of the occurrence of $PbI_2$ deintercalation at 5 min dipping time.

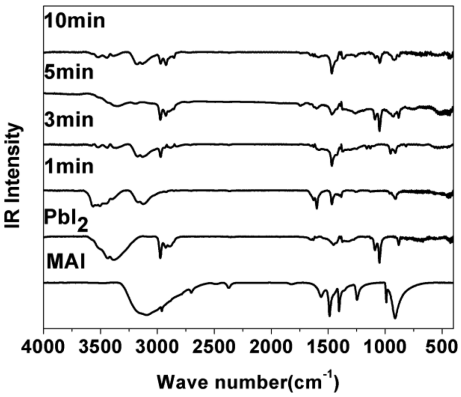


**Figure 6.** FT-IR spectra of different dipping time perovskite films obtained from a $PbI_2$ film with SVA and that of pure $PbI_2$ and MAI.

In Figure 5a, a sudden turnover of the XRD peak shift was observed with further increasing the dipping time from 5 to 10 min. Also, the FT-IR spectra in Figure 6 with 10 min dipping time show weakened IR signal from free $PbI_2$. This may reflect the formation of the $MAPbI_3$ capping layer, because deintercalated $PbI_2$ may meet the excessive MAI on the surface.

In the previous investigation, it was proposed that $PbI_2$ will become soluble in 2-propanol by formation of the $Pb_4^{2-}$,[31] i.e.,

$$CH_3NH_3PbI_3 + I^- \rightleftarrows CH_3NH_3^+ + PbI_4^{2-}$$

The $PbI_4^{2-}$ ions in 2-propanol can cocrystallize with $MA^+$ ions to grow large crystal $MAPbI_3$ on the surface, as described in the following equation:

$$PbI_4^{2-} + CH_3NH_3^+ \rightarrow CH_3NH_3PbI_3 + I^-$$

To confirm this, the scanning electron microscope (SEM) was employed to examine the surface morphology of perovskite layers. Figure 7 shows the SEM images of perovskite films prepared with different dipping times and with SVA (a−d) and without SVA (e−h). Obviously, in both cases with and without SVA, a long dipping time, i.e., 10 min, develops large perovskite nanosheets on the surface of the homogeneous cubic-shaped perovskite nanoparticles, an observation that strongly supports the above proposed mechanism of forming a perovskite capping layer on the surface after 5 min of dipping time.

**Improvement of Photovoltaic Performance by Repeated Dipping-Drying Method.** As discussed in the previous section, dipping of SVA-based $PbI_2$ in MAI solution for more than 1 min already causes deintercalation of $PbI_2$. This problem limits the exploration of the optimal $PbI_2/MAPbI_3$ composition in the active layer in the PSCs. An alternative way to optimize this composition is to shorten the dipping time of $PbI_2$ film in MAI while increasing the number of dipping-drying cycles. Figure 8 shows the J-V curves of PSCs fabricated by dipping the SVA-based $PbI_2$ in MAI for 1 min for once, twice, 3 times, and 4 times. Between each time of dipping, the reaction of $PbI_2$ with MAI in the film was immediately stopped by drying the film quickly with air flow after each dipping process. Table 3 lists the relevant parameters obtained from Figure 8. By repeating the dipping-drying cycles for 3 times, the PCE of the compact layer free PSC was significantly improved to 11.4% with a $J_{sc}$= 17.5 mA/$cm^2$, a $V_{oc}$= 1.03 V, and a FF = 0.63. Also, the $J_{sc}$ value of the best PSC is in good agreement with the integrated incident photon-to-current conversion efficiency (IPCE) in the inset of Figure 8. This high PCE value is comparable to the state-of-the-art results reported for compact

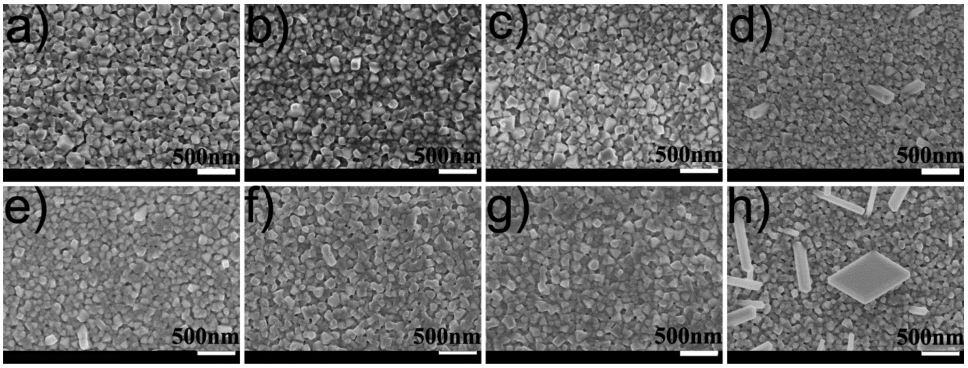


**Figure 7.** SEM images of an ITO/$MAPbI_3$ thin film obtained from the $PbI_2$ film with SVA with different dipping times: (a) 1 min, (b) 3 min, (c) 5 min, (d) 10 min and that without SVA with different dipping times: (e) 1 min, (f) 3 min, (g) 5 min, (h) 10 min.


DOI: 10.1021/acsami.5b05787
ACS Appl. Mater. Interfaces 2015, 7, 18156−18162

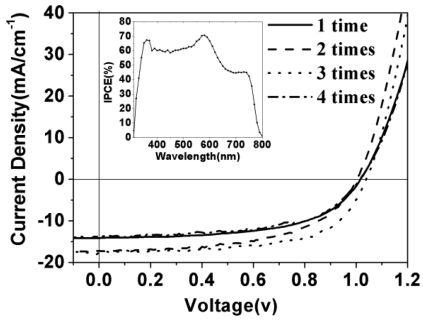


**Figure 8.** J-V curve of the ITO/perovskite/spiro-OMeTAD/Ag devices based on an SVA-$PbI_2$ layer with 1 min of dipping with different times of the repeating process. IPCE spectrum (inset) corresponds to the best PSC made from 3 times of repeating dipping-drying processes.

**Table 3. Photovoltaic Performance of PSCs Based on SVA-$PbI_2$ with Dipping in MAI for 1 min with Different Repeating Times**

| Repeating times | $J_{sc}$ (mA/cm$^2$) | $V_{oc}$ (V) | FF | PCE (%) |
|---|---|---|---|---|
| 1 | 13.9 | 1.01 | 0.60 | 8.4 |
| 2 | 17.2 | 1.00 | 0.56 | 9.6 |
| 3 | 17.5 | 1.03 | 0.63 | 11.4 |
| 4 | 13.7 | 1.01 | 0.59 | 8.1 |

layer free PSCs.[33] Importantly, the $V_{oc}$ value is more or less similar in all PSCs, indicating crystallite doping in both $PbI_2$ and $MAPbI_3$ is no longer present.

## CONCLUSIONS

In summary, we could answer the questions addressed in the Introduction: (1) Although the SVA-based $PbI_2$ is robust against reaction with MAI, resulting in $PbI_2$/$MAPbI_3$ core–shell structure in the PSC cells, increasing the dipping time in MAI solution still results in reduced photovoltaic performance. (2) The performance reduction upon prolonged dipping time of SVA-$PbI_2$ in MAI could be attributed to two detrimental events; i.e., increasing the dipping time from 1 to 5 min causes band doping in both $PbI_2$ and $MAPbI_3$ layers, and increasing it and from 5 to10 min induces recrystallization of the $MAPbI_3$ capping layer on the perovskite layer surface. (3) The photovoltaic performance was improved by an alternative repeatable dipping-drying method. By repeatedly dipping the SVA-$PbI_2$ in MAI for 1 min for 3 times, a highest PCE of 11.4% was achieved under the AM 1.5 (100 mW cm$^{-2}$) simulated sunlight illumination. This study not only discovers an important mechanism that causes the reduction of photovoltaic performance in the sequential deposition method but also simultaneously provides a solution for future development of PSCs with SVA-based $PbI_2$ precursors.

## AUTHOR INFORMATION

### Corresponding Authors

*E-mail: xf_wang@jlu.edu.cn (X.-F. Wang).
*E-mail: wjtian@jlu.edu.cn (W. Tian).

### Notes

The authors declare no competing financial interest.

## ACKNOWLEDGMENTS

This work was supported by 973 Program (2014CB643506), the Natural Science Foundation of China (no. 21221063), Program for Chang Jiang Scholars and Innovative Research Team in University (no. IRT101713018), the Graduate Innovation Fund of Jilin University (450060503118), and the Open Project of State Key Laboratory of Supramolecular Structure and Materials (no. sklssm2015019). X.-F.W. and T.M. acknowledge the support from the Japan Science and Technology Agency (JST) Advanced Low Carbon Technology R&D program (ALCA).

## ABBREVIATIONS

SVA, solvent vapor anneal; MAI, $CH_3NH_3I$; $MAPbI_3$, $CH_3NH_3PbI_3$

## REFERENCES

(1) Kojima, A.; Teshima, K.; Shirai, Y.; Miyasaka, T. Organometal Halide Perovskites as Visible-Light Sensitizers for Photovoltaic Cells. *J. Am. Chem. Soc.* **2009**, *131*, 6050–6051.
(2) Kim, H. S.; Lee, C. R.; Im, J. H.; Lee, K. B.; Moehl, T.; Marchioro, A.; Moon, S. J.; Humphry-Baker, R.; Yum, J. H.; Moser, J. E.; Grätzel, M.; Park, N. G. Lead Iodide Perovskite Sensitized All-Solid-State submicron Thin Film Mesoscopic Solar Cell with Efficiency Exceeding 9%. *Sci. Rep.* **2012**, *2*, 591–598.
(3) Lee, M. M.; Teuscher, J.; Miyasaka, T.; Murakami, T. N.; Snaith, H. J. Efficient Hybrid Solar Cells Based on Meso-Superstructured Organometal Halide Perovskites. *Science* **2012**, *338*, 643–647.
(4) Heo, J. H.; Im, S. H.; Noh, J. H.; Mandal, T. N.; Lim, C.-S.; Chang, J. A.; Lee, Y. H.; Kim, H.-j.; Sarkar, A.; Nazeeruddin, M. K.; Grätzel, M.; Seok, S. I. Efficient Inorganic–Organic Hybrid heterojunction Solar Cells Containing Perovskite Compound and Polymeric hole conductors. *Nat. Photonics* **2013**, *7*, 486–491.
(5) Burschka, J.; Pellet, N.; Moon, S. J.; Humphry-Baker, R.; Gao, P.; Nazeeruddin, M. K.; Grätzel, M. Sequential Deposition as a Route to High-Performance Perovskite-Sensitized Solar Cells. *Nature* **2013**, *499*, 316–319.
(6) Liu, M.; Johnston, M. B.; Snaith, H. J. Efficient Planar Heterojunction Perovskite Solar Cells by Vapour Deposition. *Nature* **2013**, *501*, 395–398.
(7) Miyasaka, T.; Perovskite Photovoltaics. Rare Functions of Organo Lead Halide in Solar Cells and Optoelectronic Devices. *Chem. Lett.* **2015**, *44*, 720–729.
(8) Yang, W. S.; Noh, J. H.; Jeon, N. J.; Kim, Y. C.; Ryu, S.; Seo, J.; Seok, S. I. High-Performance Photovoltaic Perovskite Layers Fabricated Through Intramolecular Exchange. *Science* **2015**, *348*, 1234.
(9) Seo, J.; Park, S.; Chan Kim, Y.; Jeon, N. J.; Noh, J. H.; Yoon, S. C.; Seok, S. I. Benefits of Very Thin PCBM and LiF Layers for Solution-Processed p–i–n Perovskite Solar Cells. *Energy Environ. Sci.* **2014**, *7*, 2642–2646.
(10) Wu, Y.; Islam, A.; Yang, X.; Qin, C.; Liu, J.; Zhang, K.; Peng, W.; Han, L. Retarding the Crystallization of $PbI_2$ for Highly Reproducible Planar-Structured Perovskite Solar Cells via Sequential Deposition. *Energy Environ. Sci.* **2014**, *7*, 2934–2938.
(11) Snaith, H. J. Perovskites: The Emergence of a New Era for Low-Cost, High-Efficiency Solar Cells. *J. Phys. Chem. Lett.* **2013**, *4*, 3623–3630.
(12) Grätzel, M. The Light and Shade of Perovskite Solar Cells. *Nat. Mater.* **2014**, *13*, 838–842.
(13) Liu, D.; Kelly, T. L. Perovskite Solar Cells with a Planar Heterojunction Structure Prepared Using Room-Temperature Solution Processing Techniques. *Nat. Photonics* **2013**, *8*, 133–138.
(14) Shi, J.; Luo, Y.; Wei, H.; Luo, J.; Dong, J.; Lv, S.; Xiao, J.; Xu, Y.; Zhu, L.; Xu, X.; Wu, H.; Li, D.; Meng, Q. Modified Two-Step Deposition Method for High-Efficiency $TiO_2$/$CH_3NH_3PbI_3$ Heterojunction Solar Cells. *ACS Appl. Mater. Interfaces* **2014**, *6*, 9711–9718.
(15) Song, J.; Bian, J.; Zheng, E.; Wang, X.-F.; Tian, W.; Miyasaka, T. Efficient and Environmentally Stable Perovskite Solar Cells Based on ZnO Electron Collection Layer. *Chem. Lett.* **2015**, *44*, 610–612.


DOI: 10.1021/acsami.5b05787
*ACS Appl. Mater. Interfaces* 2015, 7, 18156–18162

(16) Liu, D.; Yang, J.; Kelly, T. L. Compact Layer Free Perovskite Solar Cells with 13.5% Efficiency. *J. Am. Chem. Soc.* **2014**, *136*, 17116−17122.
(17) Yuan, Y.; Giri, G.; Ayzner, A. L.; Zoombelt, A. P.; Mannsfeld, S. C.; Chen, J.; Nordlund, D.; Toney, M. F.; Huang, J.; Bao, Z. Ultra-high mobility transparent organic thin film transistors grown by an off-centre spin-coating method. *Nat. Commun.* **2014**, *5*, 3005−3013.
(18) Chen, Q.; Zhou, H.; Hong, Z.; Luo, S.; Duan, H. S.; Wang, H. H.; Liu, Y.; Li, G.; Yang, Y. Planar Heterojunction Perovskite Solar Cells via Vapor-Assisted Solution Process. *J. Am. Chem. Soc.* **2014**, *136*, 622−625.
(19) Gao, C.; Liu, J.; Liao, C.; Ye, Q.; Zhang, Y.; He, X.; Guo, X.; Mei, J.; Lau, W. Formation of Organic−Inorganic Mixed Halide Perovskite Films by Thermal Evaporation of $PbCl_2$ and $CH_3NH_3I$ Compounds. *RSC Adv.* **2015**, *5*, 26175−26180.
(20) Xiao, Z.; Dong, Q.; Bi, C.; Shao, Y.; Yuan, Y.; Huang, J. Solvent Annealing of Perovskite-Induced Crystal Growth for Photovoltaic-Device Efficiency Enhancement. *Adv. Mater.* **2014**, *26*, 6503−6509.
(21) Liang, P. W.; Liao, C. Y.; Chueh, C. C.; Zuo, F.; Williams, S. T.; Xin, X. K.; Lin, J.; Jen, A. K. Additive Enhanced Crystallization of Solution-Processed Perovskite for Highly Efficient Planar-Heterojunction Solar Cells. *Adv. Mater.* **2014**, *26*, 3748−3754.
(22) Xie, F. X.; Zhang, D.; Su, H.; Ren, X.; Wong, K. S.; Grätzel, M.; Choy, W. C. Vacuum-Assisted Thermal Annealing of $CH_3NH_3PbI_3$ for Highly Stable and Efficient Perovskite Solar Cells. *ACS Nano* **2015**, *9*, 639−646.
(23) Dualeh, A.; Tétreault, N.; Moehl, T.; Gao, P.; Nazeeruddin, M. K.; Grätzel, M. Effect of Annealing Temperature on Film Morphology of Organic-Inorganic Hybrid Perovskite Solid-State Solar Cells. *Adv. Funct. Mater.* **2014**, *24*, 3250−3258.
(24) Chen, Q.; Zhou, H.; Song, T. B.; Luo, S.; Hong, Z.; Duan, H. S.; Dou, L.; Liu, Y.; Yang, Y. Controllable Self-induced Passivation of Hybrid Lead Iodide Perovskites toward High Performance Solar Cells. *Nano Lett.* **2014**, *14*, 4158−4163.
(25) Cao, D. H.; Stoumpos, C. C.; Malliakas, C. D.; Katz, M. J.; Farha, O. K.; Hupp, J. T.; Kanatzidis, M. G. Remnant $PbI_2$, an Unforeseen Necessity in High-Efficiency Hybrid Perovskite-based Solar Cells? *APL Mater.* **2014**, *2*, 091101−091106.
(26) Song, J.; Zheng, E.; Bian, J.; Wang, X.-F.; Tian, W.; Sanehira, Y.; Miyasaka, T. Low-Temperature $SnO_2$-based Electron Selective Contact for Efficient and Stable Perovskite Solar Cells. *J. Mater. Chem. A* **2015**, *3*, 10837−10844.
(27) Zhao, Y.; Zhu, K. Three-Step Sequential Solution Deposition of $PbI_2$-Free $CH_3NH_3PbI_3$ Perovskite. *J. Mater. Chem. A* **2015**, *3*, 9086−9091.
(28) Patterson, A. L. The Scherrer Formula for X-Ray Particle Size Determination. *Phys. Rev.* **1939**, *56*, 978−982.
(29) Zhou, Y.; Yang, M.; Vasiliev, A. L.; Garces, H. F.; Zhao, Y.; Wang, D.; Pang, S.; Zhu, K.; Padture, N. P. Growth Control of Compact $CH_3NH_3PbI_3$ Thin Films via Enhanced Solid-State Precursor Reaction for Efficient Planar Perovskite Solar Cells. *J. Mater. Chem. A* **2015**, *3*, 9249−9256.
(30) Chiang, C.-H.; Tseng, Z.-L.; Wu, C.-G. Planar Heterojunction Perovskite/$PC_{71}BM$ Solar Cells with Enhanced Open-Circuit Voltage via a (2/1)-Step Spin-Coating Process. *J. Mater. Chem. A* **2014**, *2*, 15897−15903.
(31) Yang, S.; Zheng, Y. C.; Hou, Y.; Chen, X.; Chen, Y.; Wang, Y.; Zhao, H.; Yang, H. G. Formation Mechanism of Freestanding $CH_3NH_3PbI_3$ Functional Crystals: In Situ Transformation vs Dissolution−Crystallization. *Chem. Mater.* **2014**, *26*, 6705−6710.
(32) Preda, N.; Mihut, L.; Baibarac, M.; Baltog, I.; Ramer, R.; Pandele, J.; Andronescu, C.; Fruth, V. Films and Crystalline Powder of $PbI_2$ Intercalated with Ammonia and Pyridine. *J. Mater. Sci.: Mater. Electron.* **2009**, *20*, 465−470.
(33) Ke, W.; Fang, G.; Wan, J.; Tao, H.; Liu, Q.; Xiong, L.; Qin, P.; Wang, J.; Lei, H.; Yang, G.; Qin, M.; Zhao, X.; Yan, Y. Efficient Hole-Blocking Layer-Free Planar Halide Perovskite Thin-Film Solar Cells. *Nat. Commun.* **2015**, *6*, 6700−6706.


DOI: 10.1021/acsami.5b05787
*ACS Appl. Mater. Interfaces* 2015, 7, 18156−18162